ELSEVIER

Journal of Fluids and Structures 21 (2005) 707–730

JOURNAL OF FLUIDS AND STRUCTURES

www.elsevier.com/locate/jfs

An investigation on the lift force of a wing pitching in dynamic stall for a comfort control vessel

E. Hoo, K.D. Do, J. Pan*

School of Mechanical Engineering, University of Western Australia, Crawley, WA 6009, Australia

Received 1 November 2004; accepted 11 August 2005
Available online 20 October 2005

Abstract

On the basis of a comfort control system for ocean vessels, the control forces and moments in the form of lift forces from active wings are of important interest. In an ocean vessel comfort control system, active wings or fins are commonly used and constantly adjust their angles of attack to produce optimal sea-keeping conditions. The unsteady nature of the flow field around a wing, and the behaviour of the generated lift force must be understood in order to optimize the comfort control system. This paper presents experimental data on the flow past a pitching wing, paying particular attention to the lagging effects between the fluid dynamic lift force and the motion of the wing at large angles of attack as a function of peak angle of attack and reduced frequency of oscillation. The range of motion investigated has been chosen according to the applicability of a comfort control wing surface. Numerical data is also included to aid explanation on some of the witnessed phenomena.
© 2005 Elsevier Ltd. All rights reserved.

Keywords: Hydrodynamic lift; Dynamic stall; Time delay; Comfort control; Wing; Fin

1. Introduction

One of the earliest contributions to the field of unsteady fluid dynamics of a pitching wing is by Theodorsen (1935), who considered a flat plate and a trailing flat wake of vorticity in an incompressible fluid for a two-dimensional (2-D) thin airfoil. Theodorsen found that the lifting force on a thin aerofoil comprised two components. A noncirculatory component which includes added mass effects, and a circulatory component which includes forces arising from the bound vortex system. These two force components were determined by finding the velocity potential associated with the circulatory and noncirculatory flow around the wing, and then deriving the pressure difference across the wing chord from this potential. With the assumption of simple harmonic pitching motion, Theodorsen showed that a relatively simple function could be used to modify the known steady state solution for the wing lift to give an analytical solution for the unsteady wing lift. However, the Theodorsen model assumes a 2-D wing, and the ideal Kutta condition of regular flow at the trailing edge. It is therefore expected that substantial errors in the Theodorsen model would exist at high peak angles of attack and high reduced frequencies of oscillation—where the Kutta condition is known to break down.

*Corresponding author. Tel: +618 6488 3600; fax: +618 6488 1024.
E-mail addresses: erich@mech.uwa.edu.au (E. Hoo), duc@mech.uwa.edu.au (K.D. Do), pan@mech.uwa.edu.au (J. Pan).

0889-9746/$ - see front matter © 2005 Elsevier Ltd. All rights reserved.
doi:10.1016/j.jfluidstructs.2005.08.009

To account for the three-dimensional (3-D) effect during the starting lift, Jones (1939, 1941) considered the unsteady lift of a finite wing. Jones utilized a model on the lift force after a sudden jump of angle of attack in the 2-D case. In Jones' model, superposition is used by breaking the given motion down into a succession of small jumps, and summing the lifting effects associated with each step. Under this principle, a general solution was derived giving the instantaneous lift for any combined vertical and oscillatory motion. To account for 3-D effects, Jones applied a correction to the incident angle of attack by finding the downwash at the leading edge of the wing. It was concluded that the correction approached Prandtl's lifting line theory for a long trailing wake.

With the increasing use of helicopters for military use from the 1950s, greater efforts were aimed at increasing the efficiency of helicopter blades. Helicopter blades would experience periodic stalling and un-stalling, limiting the forward speed of the helicopter. This was attributed to large torsional oscillations of the blades. It had long been observed that a pitching wing would continue producing lift at angles of attack much greater than the static stall angle before stalling. This phenomenon known as dynamic stall has been studied extensively both experimentally and numerically. Early studies on dynamic stall found in Ericsson and Reding (1972) were based on a quasi-steady theory that required static experimental data as an input for dynamic stall predictions.

McCroskey (1973) studied the inviscid flow-field of an unsteady airfoil with particular focus on the dynamic stall region. Theodorsen's analysis of the velocity potential in the unsteady wake of an oscillating wing was combined with velocity potentials associated with thickness, camber and angle of attack to find the pressure distribution around the wing. It was concluded that the assumption of inviscid flow correctly predicted boundary layer separation, but not the behaviour of the lift above static stall.

A review by McCroskey (1982) provides useful physical interpretations of dynamic stall. McCroskey summarizes that due to the large hysteresis effects, the maximum values of lift, drag and moment can greatly exceed the maximum static counterparts. It is also mentioned that in some parts of the cycle of motion, negative damping effects are observed implying the force generated can be greater at a particular angle of attack due to damping effects than the force generated at a higher angle of attack. The physical behaviour of the flow around the wing is described leading up to, and during, dynamic stall.

Realizing the inaccuracy of inviscid models for the analysis of dynamic stall, several authors have developed semi-empirical models from experimental data. Tran and Petot (1981) developed the ONERA semi-empirical model for 2-D dynamic stall of an airfoil. This model applied curve fitting to experimental data to describe the aerodynamic forces as a function of the variables describing the motion of the wing. Bielawa et al. 1983 also developed a semi-empirical model that describes the fluid dynamic forces from the pitch and pitch rate of the wing.

More recently, the advancement in computing power has motivated the use of computational fluid dynamics to observe vortex generation and vortex patterns in the dynamic stall region. In Akbari and Price (1999) the incompressible viscous flow over 2-D elliptic airfoils oscillating in pitch at large angles of attack, at a Reynolds number of 3000 is numerically simulated using a vortex method. The main focus of their simulation was to investigate the effects of frequency of oscillation, mean angle of attack, location of pitch axis and the thickness ratio of the airfoil, on the flow pattern. A vortex method was used to solve the 2-D Navier–Stokes equations in vorticity/stream-function form using a time marching approach. Although physical experiments were not performed, simulated results were compared with available data. It was concluded there that the reduced frequency had the most influence on the resulting flow field.

In Akbari and Price (2003) the same numerical method used in Akbari and Price (1999) was used to simulate the flow over a pitching NACA 0012 airfoil at a Reynolds number of 10^4. Once again, the reduced frequency of oscillation was concluded as the most influential parameter for the flow field. It is noted in both papers by Akbari and Price that the numerical method used was limited to a laminar regime, and would not be accurate for Reynolds numbers higher than 10^4.

The development of Particle Image Velocimetry (PIV) has also improved the ability to investigate dynamic stall. In Wernet et al. (1996), PIV is used to experimentally investigate the flow field around an airfoil pitching under deep dynamic stall conditions. It was found that the flow field exhibited strong nonreproducibility in terms of vortex structure geometry during oscillation cycles. It was also found that the nonreproducibility was highly dependent on the reduced frequency of oscillation.

All the aforementioned studies on dynamic stall have been motivated by the helicopter industry. As a result, the wing motions investigated typically have a mean angle of attack, $\bar{\alpha}$ greater than 10°, and a superimposed pitch oscillation of approximately $\pm 15^\circ$. A study on the flow past a wing used as part of a comfort control system implies an investigation of a different range of pitching motion. A comfort control system increases the stability of an ocean vessel subject to environmental disturbances by producing stabilizing roll moments to reduce or attenuate the vessel's roll and pitch displacement. Control actuators for such systems can vary from anti-roll tanks, and moving mass systems, to interceptors and submersed wings. The submersed wing is one of the most common control surfaces, and will be the focus of this paper. Two wings, one fitted to each side of the vessel's hull can generate a stabilizing roll moment by

producing lift forces in opposite directions. This implies that $\bar{\alpha}$ is set at 0° for each wing, and results concluded by previous studies may not entirely represent the flow field in this case. Furthermore, emphasis in this study is placed more on the generated lift force and its phase difference with the angle of attack rather than the generated vortex pattern.

An investigation into the lifting force of a pitching wing is therefore motivated by the need to improve a comfort control system. The dynamics of the generated lift force from a wing can affect the control model significantly, even for the case without disturbances. The problem can be explained with the state–space model below (Do and Pan, 2001):

$$\begin{aligned} \dot{x}_1 &= x_2, \\ \dot{x}_2 &= f_1(x_1, x_2) + kL, \\ \dot{\alpha} &= \omega, \\ \dot{\omega} &= f_2(\alpha, \omega) + u, \end{aligned} \tag{1}$$

where x_1 and x_2 represent the roll displacement and the roll velocity of a vessel, while α and ω are the angle of attack and angular velocity of the wing, respectively; f_1 and f_2 are functions determined by the dynamics of the vessel and wing, such that $f_1(0, 0) = 0$, and $f_2(0, 0) = 0$, k is a constant, L is the lift force produced by the wing, and u is the control input.

If the popular control methods are followed to attenuate the roll motion of the boat, L is designed as an immediate control input. This control will be of the form $L = v(x_1, x_2)$ such that $\lim_{x_1,x_2\to 0} v(x_1, x_2) = 0$. Internal dynamic problems may arise since L depends on the dynamics of the wing. If $L = \gamma\alpha$ where γ is a constant, the system represents a cascade structure [see Krstic et al. (1995)] and is in a form convenient for control design. However, if the force is also affected by the velocity or the frequency of oscillation, for example $L = \gamma_1\alpha + \gamma_2\omega$, where γ_1 and γ_2 are both constants, the zero/internal dynamics of the system may become unstable. This phenomenon can be explained as follows. We have;

$$v(x_1, x_2) = 0, \quad L = \gamma_1\alpha + \gamma_2\omega = 0;$$

since $\dot{\alpha} = \omega$, we have

$$\dot{\alpha} = -\frac{\gamma_1}{\gamma_2}\alpha. \tag{2}$$

It is seen that Eq. (2) becomes unstable if γ_1/γ_2 is a negative number. Furthermore, if the force L is also a function of $\dot{\omega}$, additional complications are introduced, and the control input u will also appear in the vessel's roll dynamics. The system will no longer be of a cascade structure, which is crucial for employing the established control design techniques (Khalil, 1996).

Another complication for comfort control may be caused by lagging effects in the forcing function of the wing. If the lift force is simply represented by $L = k_3\alpha(t - \eta)$, where k_3 is a constant and η represents a time delay constant, the system dynamics become

$$\begin{aligned} \dot{x}_1 &= x_2, \\ \dot{x}_2 &= f_1(x_1, x_2) + k_3\alpha(t - \eta), \\ \dot{\alpha} &= \omega, \\ \dot{\omega} &= f_2(\alpha, \omega) + u. \end{aligned} \tag{3}$$

Here, the task becomes controlling a system with lag. Therefore, the time delay properties of the forcing function L must be investigated in order to deal with their effects on control performance.

This paper contributes extensive experimental data on the lift force of a pitching wing in a range of motion more applicable to a comfort control wing. The underlying goal is to understand the dynamics of the lift force, or the parameter L in system (3), and therefore provide a direction to improving a comfort control system. The new experimental data has revealed identifiable trends in the phase difference between the lift force and the angle of attack. The data also indicates that dynamic stall mechanisms used to describe hydrodynamic phenomena over a different range of pitching motion can also be used to describe the lifting characteristics witnessed here.

The rest of the paper is organized as follows: Section 2 outlines the Theodorsen model to be used for comparing unsteady lift characteristics with experimental results. Comparison between the 2-D model and 3-D experimental results are addressed by making corrections to the 2-D model to approximate 3-D effects. The experimental set-up is presented with details of the physical rig and data acquisition in Section 3. Finally, Section 4 compares and analyses the results to assess the phase difference and dynamic stall characteristics of the lifting force.

Appendix A presents computational fluid dynamic (CFD) data that aids the explanation on several of the observed phenomena related to the lift force. The CFD procedure is briefly addressed in terms of the mesh structure, and boundary conditions used in numerical simulations. The numerical results are validated by comparison to the experimental results before pressure contours are presented to analyse the flow around the wing.

2. Mathematical model

2.1. Thin airfoil theory

In order to improve the mathematical model for a comfort control system (2), the lift force L must also be modelled. More recently developed semi-empirical models offer a good comparison with experimental data. However, it would be more meaningful, and useful from a control modelling perspective to utilize a model derived from physical flow relationships.

Comparing a theoretical model with numerical or experimental results would allow a better understanding of the physical flow. Discrepancies arising from comparisons could possibly be identified with a certain aspect or assumptions contained within the model. This would not be possible with a model based on experimental curve fitting.

For these reasons, the unsteady hydrodynamic forces are approximated using Theodorsen's approach as described in the previous introductory section. For clarity, and to aid with experimental comparisons later, the assumptions of Theodorsen's model are listed below.

(i) The model assumes a 2-D flow field which will be corrected using Prandtl's lifting line theory to account for 3-D downwash effects. The correction will be calculated at the peak angle of attack. This correction will define new limits to the oscillatory motion. Following an analysis of Eq. (5d), this method was found to have little bearing on the phase difference and more effect on the peak magnitude of the lift force since Prandtl's 3-D correction will only affect the peak angle of attack and not the frequency of oscillation. Furthermore, in the calculation of the superimposed downwash, an elliptic spanwise circulation distribution has been assumed. This was attempted despite the low span to chord aspect ratio to allow initial comparisons between experimental results and theoretical predictions. The favourable results dissuaded investigation of a more complex comparative method.

(ii) The wing is approximated by a flat plate. This gives a fairly good approximation since the wing geometry will only affect the noncirculatory velocity potential component. Calculation of the circulatory component, or the velocity potential due to the unsteady wake depends only on the wing motion and is independent of the wing geometry (McCroskey, 1973).

(iii) The Kutta condition is assumed at the trailing edge. This implies regular flow in the vicinity of the trailing edge with the wake assumed to be thin and straight. This assumption is necessary to solve for the velocity potential due to the circulatory flow.

(iv) The vortex sheet is comprised only of vortices shed from the wing's trailing edge. This implies that *dynamic stall* vortices shed from the leading edge of the wing during large angles of attack are not taken into account.

(v) Simple harmonic pitching motion of the wing is assumed. Environmental disturbances at sea can be approximated by regular wave disturbances. The motion of the comfort control wings would therefore also be approximately simply harmonic.

In order to find the lifting force on a wing, the objective is to find the pressure difference Δp between the upper and lower surface of a thin airfoil or wing section as a function of the velocity potential φ. This relationship can be derived from the momentum equation of a Stokesian fluid as

$$\Delta p = -2\rho\left(\frac{\partial \varphi}{\partial t} + V\frac{\partial \varphi}{\partial x}\right), \tag{4}$$

where ρ is the density of the fluid, and V is the mean velocity of the incident flow (Lamb, 1932). From Eq. (4) evaluation of the lifting force requires the evaluation of the velocity potential as a function of x along the wing surface. The basic flow around a wing can be considered as being formed by two vortices: one representing an element of circulation around the wing $\Delta\Gamma$, and one representing the shed vortex counterpart in the wake $-\Delta\Gamma$ (see Fig. 1).

By Joukowski's conformal transformation (see Fig. 2), streamlines of the circulatory flow can be mapped onto eccentric circles with a circle of unit radius representing the wing. With the origin at the centre of the circle, and the

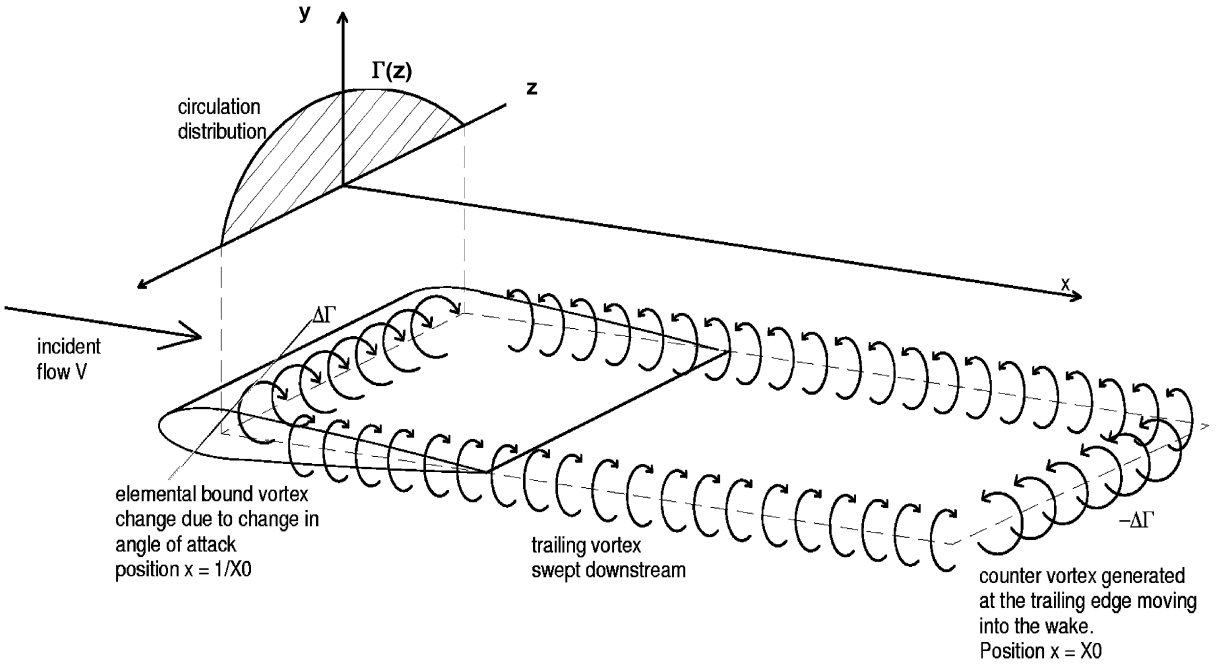

Fig. 1. 3-D representation of circulation distribution, trailing vortex, elemental circulation, and counter vortex in the wake.

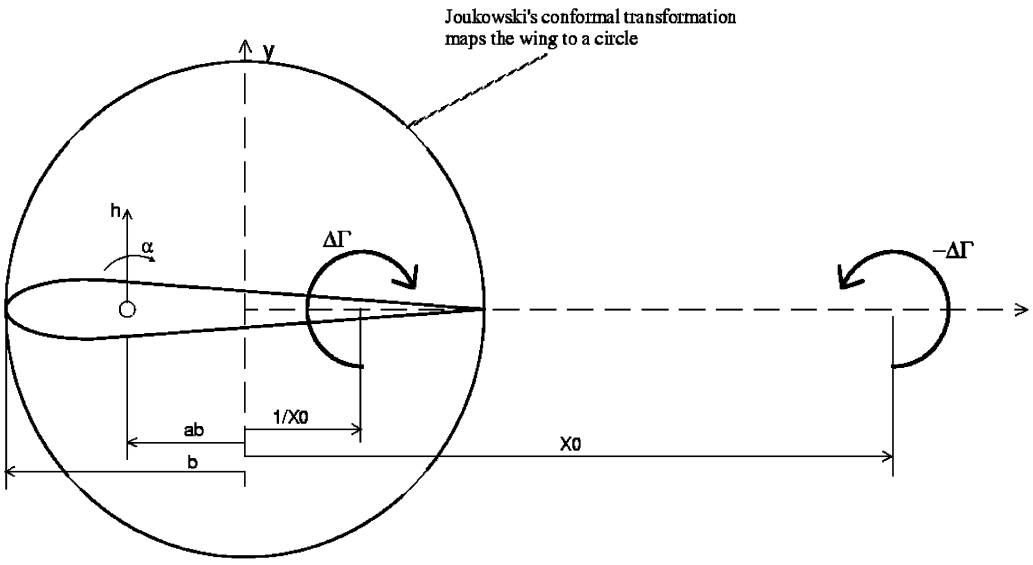

Fig. 2. Parameters of the wing following Joukowski transformation.

x-axis along the chord of the wing. A shed vortex at position $x = X_0$ means the wing bound vortex must be at position $x = 1/X_0$.

The total lift force generated by simple harmonic pitch motion $\alpha(t) = \alpha e^{j\omega t}$, with α_1 and ω the peak magnitude and circular frequency of the motion in a fluid with mean flow velocity V, can be written as a sum of the circulatory and

noncirculatory forces (Theodorsen, 1935),

$$L_{\text{total}} = L_\Gamma + L_{NC} = \pi\rho b\alpha_1\sqrt{F_0^2 + G_0^2}\, e^{j\omega(t+\phi/\omega)}, \tag{5a}$$

where

$$L_{NC} = \pi\rho b^2(V\dot{\alpha} - ab\ddot{\alpha}), \tag{5b}$$

$$L_\Gamma = -2\pi\rho Vb\left(V\alpha + \dot{\alpha}\left(\frac{1}{2} - a\right)\right)(F(k) + jG(k)), \tag{5c}$$

$$\begin{aligned} F_0 &= \omega^2 b^2 a\alpha_1 + 2V^2F(k) - 2V\omega b(\tfrac{1}{2} - a)G(k),\\ G_0 &= \omega bV\left(1 + 2F(k)(\tfrac{1}{2} - a)\right) + 2V^2G(k),\\ \phi &= \tan^{-1}\frac{G_0}{F_0}, \end{aligned} \tag{5d}$$

b is half the chord length, and ab is the position of the axis of rotation from the centre chord point. $F(k)$ and $G(k)$ are defined by an approximation to the Theodorsen function

$$C = F(k) + jG(k) = 0.5 + \frac{0.0075}{jk + 0.0455} + \frac{0.10055}{jk + 0.3}, \tag{5e}$$

where $k = \omega b/V$ is the reduced frequency. As a function of $\alpha(t)$, the total lift can be represented by

$$L_{\text{total}} = K\alpha(t - \eta), \tag{5f}$$

where $K = \pi\rho b\sqrt{F_0^2 + G_0^2}$ and $\eta = -\phi/\omega$ is the time delay.

The time delay η depends on the frequency of oscillation and physical parameters of the wing. The recognition of this time delay is important since it proves that the time difference between the lift force and the angle of attack is inherited from the momentum equations used to derive this model. Therefore, in physical systems, any observed time difference is a result of the physics of the flow around the wing *in addition* to the time delay of the sensing and actuation system. Any assumption of ignoring the delay of the flow dynamic force may lead to an error in the system modelling and a decrease in control performance.

2.2. Comparison with 3-D results

The theoretical prediction is based on 2-D assumptions. Comparison with 3-D experimental results requires some discussion of the complexities of the 3-D flow around the wing. This section however, will not attempt to define the qualitative differences between 2-D and 3-D wing flow and instead attempts to find a way to compare 2-D simulated and 3-D experimental results.

Prandtl's lifting line theory accounts for the effects of the trailing vortices from a 3-D wing by calculating a resulting downwash superimposed on the incident flow. This in effect reduces the physical angle of attack to an effective angle of attack. Jones (1941) found that when the wake is short, the flow conditions are similar to an infinite wing, since a short wake will induce negligible downwash. When the wake lengthens, the flow conditions approach the theory introduced by Prandtl. For simplicity, the initial starting lift is not considered and Prandtl's lifting line theory is used to calculate a correction to the angle of attack used in theory for comparison with 3-D experimental results.

By the Biot-Savart law (Houghton and Carpenter, 2003), a vortex tube will induce a velocity in the surrounding fluid. In the case of a finite wing, the incident velocity, V will be combined with an induced velocity due to the trailing vortices. This induced velocity w, called a downwash, effectively reduces the angle of attack of the wing by $\varepsilon = w/V$. This implies that the lifting characteristics of a section of wing of finite aspect ratio at a local angle of attack of α_1, is similar to a 2-D wing at an effective angle of attack of $(\alpha_1 - \varepsilon)$. This theory can therefore be used to determine the lifting characteristics of wings of finite span by analysing wings of infinite span. Although Prandtl's theory assumes steady flight or no pitching motion, it may still provide a starting point for comparing the 2-D and 3-D results.

With a horse-shoe vortex representation, the circulation around the wing, proportional to the lift is less at the wing tips. The actual circulation distribution along the span of the wing can be rather complicated depending on various parameters of the wing. The assumption of an elliptical distribution of circulation along the span of the wing (see Fig. 1) leads to a very simple relationship between the downwash and the peak circulation value Γ_0 (Houghton and

Carpenter, 2003)

$$w = \frac{\Gamma_0}{2s}, \tag{6}$$

where s is the wing span length. This is the simplest load expression for wing flight; however it is often a good approximation to more complicated systems. The peak circulation for an assumed elliptic distribution can be found by measuring the lift force generated (Houghton and Carpenter, 2003):

$$\Gamma_0 = \frac{L}{\frac{1}{2}\rho V \pi s} \tag{7}$$

where L is the peak lift force measured. For each experimental run at a particular peak angle of attack and reduced frequency of oscillation, the peak lift force is measured. This corresponds with the peak circulation via (7), which in turn gives the correction to the angle of attack via (6). This correction determines the new peak angle of attack used for the corresponding 2-D theoretical calculation that is simulated for comparison.

3. Description of the experiment

3.1. Experimental set-up

The experimental investigation forms the basis of designing a 'real' wing control surface to be used on a vessel. The method of actuation, supporting structures, sensor placement, data acquisition and dynamic control of the wing are all important areas that were considered in this experiment. The physical dimensions of the wing were determined with consideration of the testing rig support capabilities, the size of the tow tunnel facility, and also the size of wing required for a comfort control project vessel (5 m research vessel). For simplicity, a symmetrical NACA0012 profile was selected with associated chord length, $2b = 0.15$ m, and span $s = 0.3$ m. Axis of rotation was set at the quarter chord point (see Fig. 2: $ab = -0.0375$ m, $a = -0.5$).

The following description is based on a coordinate system with x in the flow direction, y transverse to the flow and z pointing vertically up towards the trolley.

From previous studies on the hydrodynamic lift force (Theodorsen, 1935; Jones, 1939; Akbari and Price, 1999, 2003), it is understood that the vortex formation and shedding has a great effect on the fin forces. Minimizing outside disturbances by reducing the amount of intruding supporting rods was therefore beneficial to the meaning of the results. Since the tow tank trolley lies above the water, the natural solution to this problem was to support the wing vertically by one supporting shaft, or cylinder, in line with the z-direction (see Fig. 3). This shaft was also attached to an actuator above the water and turned to adjust the angle of attack. This had another advantage in that it more accurately mimicked the true behaviour of a submersed wing attached to a ship hull.

The theoretical line of action at which the lift force acts lies at 1/4 chord length (Jones, 1939, 1941). Placing the wing shaft at 1/4 chord length minimized any moment caused by the lift force in the axially aligned direction. This had several advantages. Firstly, the force required to adjust the angle of attack was reduced. Secondly, the process required to resolve lift and drag forces to force sensor readings above the water was simplified.

The diameter of the supporting wing shaft was chosen to avoid resonance between the vortex-shedding frequency and natural bending frequency. The rigidity of its cantilevered connection to its support above was bolstered by the motor and bearing housing structure. Although the set-up provided adequate supporting strength and rigidity, it is noted that at very high lifting loads, a slight deflection was observed at the bottom wing tip.

Hydrodynamic forces applied to the vertical wing will cause moments in the y-direction (xz-plane), from drag, and in the x-direction (yz-plane) from lift. Also moments induced by turning the cylinder (to create pitch oscillation) will exist in the z-direction (xy-plane). Therefore, the moments in the x- and y-direction, containing information about the lift and drag forces were required to be measured independently of the moment generated in the z-direction. If the end of the shaft above the water is attached to a flat plate in the xy-plane, moments generated by the lift and drag forces on the vertical wing below will cause the plate to deflect in the z-direction.

Force measuring cells placed at the ends of this plate measuring vertical deflections give information about the drag and lift forces on the vertical shaft. Load cells, designed to measure strain in compression and tension only, are suitable for this purpose. A moment generated in the z-direction is not measured by the load cells, since stresses applied to the load cells in that case would be in shear.

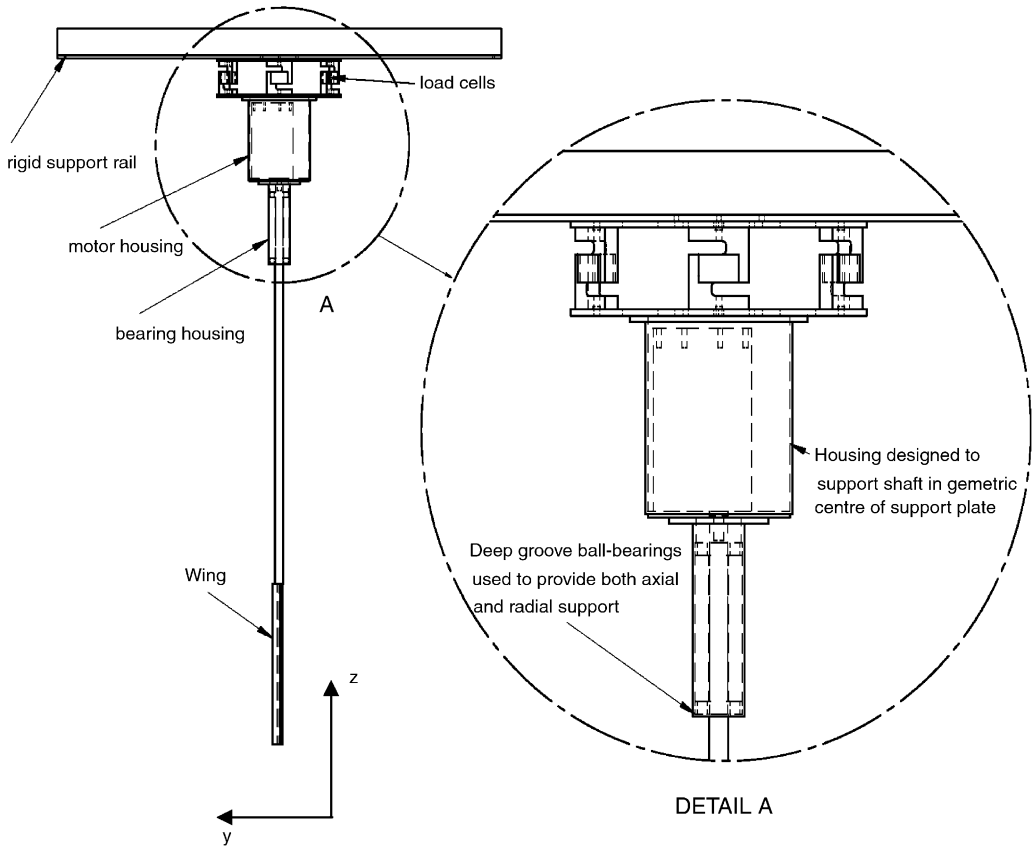

Fig. 3. Testing rig design outline.

Fig. 3 illustrates the rig designed for the experiment. The rig supports the wing vertically, and is fastened to a trolley that traverses a water tow tunnel at pre-set speeds. A DC motor connected in series with the supporting shaft provides the torque to adjust the wing's angle of attack. Lift and drag forces are resolved into vertical loads read by load cells placed above the wing on the supporting structure. The experimental rig is also equipped with a potentiometer for angular position feedback. Data is collected and processed by a 12 bit data acquisition card (NI DAQCard – 6062E). LabWindows functions is the operating software, in which the control algorithm governing the motion of the wing can be implemented.

3.2. Experimental runs

Although a flow in the region of Reynolds number, $\mathrm{Re} = 10^7$ would be representative of a real vessel travelling at common speeds, the nature of the experimental apparatus restricted the investigated flow regime to $\mathrm{Re} = 10^4$ (investigations at $\mathrm{Re} = 10^7$ are to be conducted at a future date). It should be noted that flows with Reynolds numbers around $\mathrm{Re} = 10^4$ represent a flow in transition to turbulence. This was considered with the turbulence model used in a CFD analysis presented in Appendix A. In this flow regime, the wing motions to be investigated were defined in terms of reduced frequency of sinusoidal motion, and peak angle of attack. Limits of the experimental apparatus restricted reduced frequencies to $0 < k \leqslant 0.9$ and maximum peak angles of attack to $0^\circ \leqslant \alpha_1 < 40^\circ$(with a mean angle of attack of 0°). This represents a maximum oscillatory frequency of approximately 2 Hz, which extends the investigation slightly beyond the probable maximum operating frequency of a comfort control wing (with reference to the frequency of ocean disturbances, this maximum operating frequency is approximately 1 Hz). McCroskey (1982) mentions the maximum angle of attack before deep stall in a dynamic stall regime is approximately $\alpha_1 = 20^\circ$. However, in the physical application of rudders and comfort control wings, the peak angle of attack may be as large as 35°. This made it

necessary to investigate angles of attack greater than 20°. Furthermore, the results from peak angles in excess of 20° would offer some interesting insight into the behaviour of the lift force during deep dynamic stall.

For each run, the towing rig was brought up to speed and the oscillatory motion of the wing also engaged. Lift forces were recorded when the lift cycles had attained a steady level of repeatability.

4. Experimental results and discussion

4.1. Lift coefficient

Initially the steady state lift for fixed angles of attack was experimentally measured and compared with the theoretical inviscid static lift calculated by using Theodorsen's thin airfoil theory with the assumption of no wing movement (see Fig. 4). The comparison between the two curves show the experimentally measured static lift is well below the theoretical static lift, and suggests the wing has stalled beyond an angle of attack of 10°.

For reduced frequencies varying between $0 \leqslant k \leqslant 0.9$, and oscillatory limits of $-10° \leqslant \alpha \leqslant 10°$, $-20° \leqslant \alpha \leqslant 20°$, $-30° \leqslant \alpha \leqslant 30°$ and $-40° \leqslant \alpha \leqslant 40°$ the dynamic lift force generated by the wing was measured experimentally. Using results obtained from the experimental data, the effective angle of attack was found for each experimental run. Theoretical predictions were simulated for comparison with consideration of the downwash correction. The lift coefficient is defined as $C_L = L/\frac{1}{2}\rho V^2 A$, where A is the wing's reference area. C_L and the angle of attack α, with reduced time t/T, T being the period, are presented in Figs. 5–8 along with hysteresis plots. Angle of attack α is labelled as AOA in all plots to follow.

Ignoring the noise embedded in the measured readings (a result of the sensing apparatus and the imperfect towing rig), Fig. 5 plots the lift coefficient against time revealing almost smooth sinusoidal variation with reduced time, and high repeatability between cycles. This is expected since the wing is oscillating within the static stall limits, and the flow is therefore expected to remain attached throughout the pitching cycle.

Increasing k widens the hysteresis loops indicating a larger phase difference with the angle of attack. Also an increase in k brings about a slightly higher coefficient of lift—greater than the steady lift generated at a fix angle of attack (see Fig. 4). Theodorsen's predictions at low k appear to overestimate the magnitude of the lift. Theodorsen's model also predicts a small lag of the lift force behind the angle of attack, while experimental results approximate a small lead of the lift force over the angle of attack. As k increases, theoretical and experimental results reach a closer agreement in terms of phase and magnitude up to a value of k when Theodorsen's model underestimates the magnitude of the lift force, and overestimates the lead of the lift over the angle of attack. This lead at large values of k becomes so high that the sign of the lift force becomes opposite to the sign of the angle of attack during the latter part of the return stroke. This indicates that the wing is extracting energy from the fluid. Although the pitching moment coefficient is not measured, it can still be concluded that the net damping in the pitching moment loop has become negative.

With the peak angle of attack raised to $\pm 20°$ and $\pm 30°$ (see Figs. 6 and 7), the wing is now oscillating beyond the static stall limit found experimentally to be approximately 15° for this wing. Inspection of the experimental results at low values of k reveals the onset of stall at approximately 19° for $\pm 20°$ peak angle of attack and 27° for $\pm 30°$ peak angle of attack. This is also evident in the hysteresis loop where the lift plateaus slightly as it approaches 20°. By

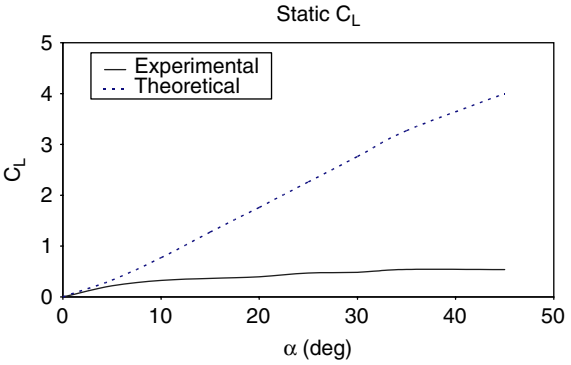

Fig. 4. Steady state lift coefficient measured at fixed angles of attack compared with theoretical inviscid static lift. Lift recorded when readings attained steady state. Comparison of the curves show the wing has stalled beyond and angle of attack of 10°.

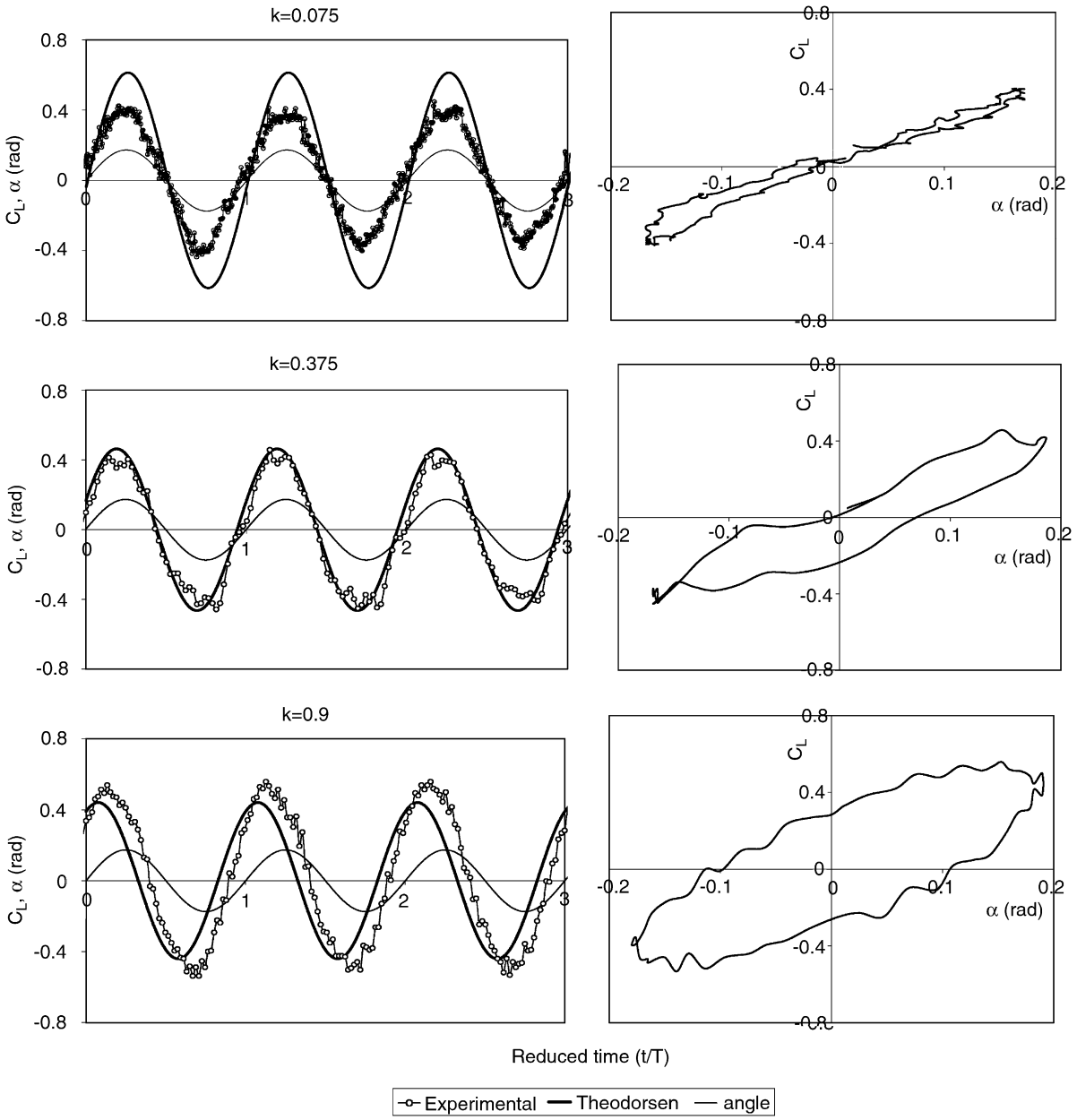

Fig. 5. Lift force measured for $0 \leqslant k \leqslant 0.9$, $-10^\circ \leqslant \alpha \leqslant 10^\circ$, $\mathrm{Re} = 10^4$. Left-hand side—against reduced time, Right-hand side—hysteresis plots (clockwise orientation).

increasing k up to 0.3, the stall is delayed and the lift increases all the way to the peak angle of attack. The lift curve plotted against reduced time as well as the hysteresis loop exhibits a smoother trend with less apparent unsteady deflections. Beyond $k = 0.4$, hysteresis effects become more apparent. Hysteresis loops are much wider, and the phase lead of the lift over the angle of attack increases at a greater rate. In Akbari and Price (2003), similar observations were made by simulating vorticity snap-shots of a pitching wing. It was found that at low values of k, leading edge or 'dynamic stall' vortices shed before the maximum angle of attack was reached. Suction effects from vortices shed and moving along the surface of the wing also affected the lift force during the return cycle of motion. This has been observed here at $k = 0.075$ with the apparent stall just before maximum angle of attack followed by a recovery of lift during the return stroke. At higher values of k, Akbari and Price observed that faster motion of the wing meant the

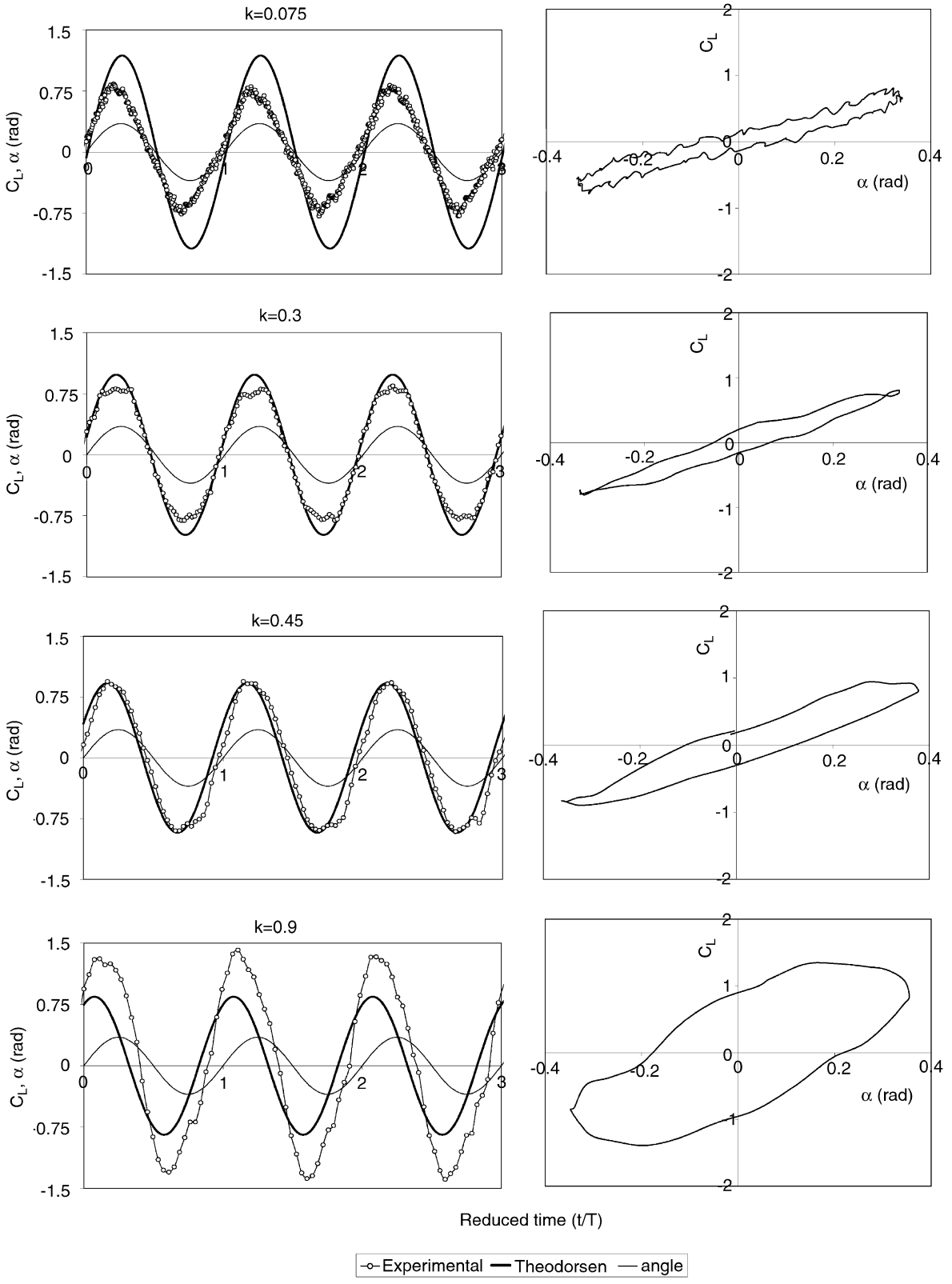

Fig. 6. Lift force measured for $0 \leqslant k \leqslant 0.9$, $-20^\circ \leqslant \alpha \leqslant 20^\circ$, $\mathrm{Re} = 10^4$. Left-hand side—against reduced time, Right-hand side—hysteresis plots (clockwise orientation).

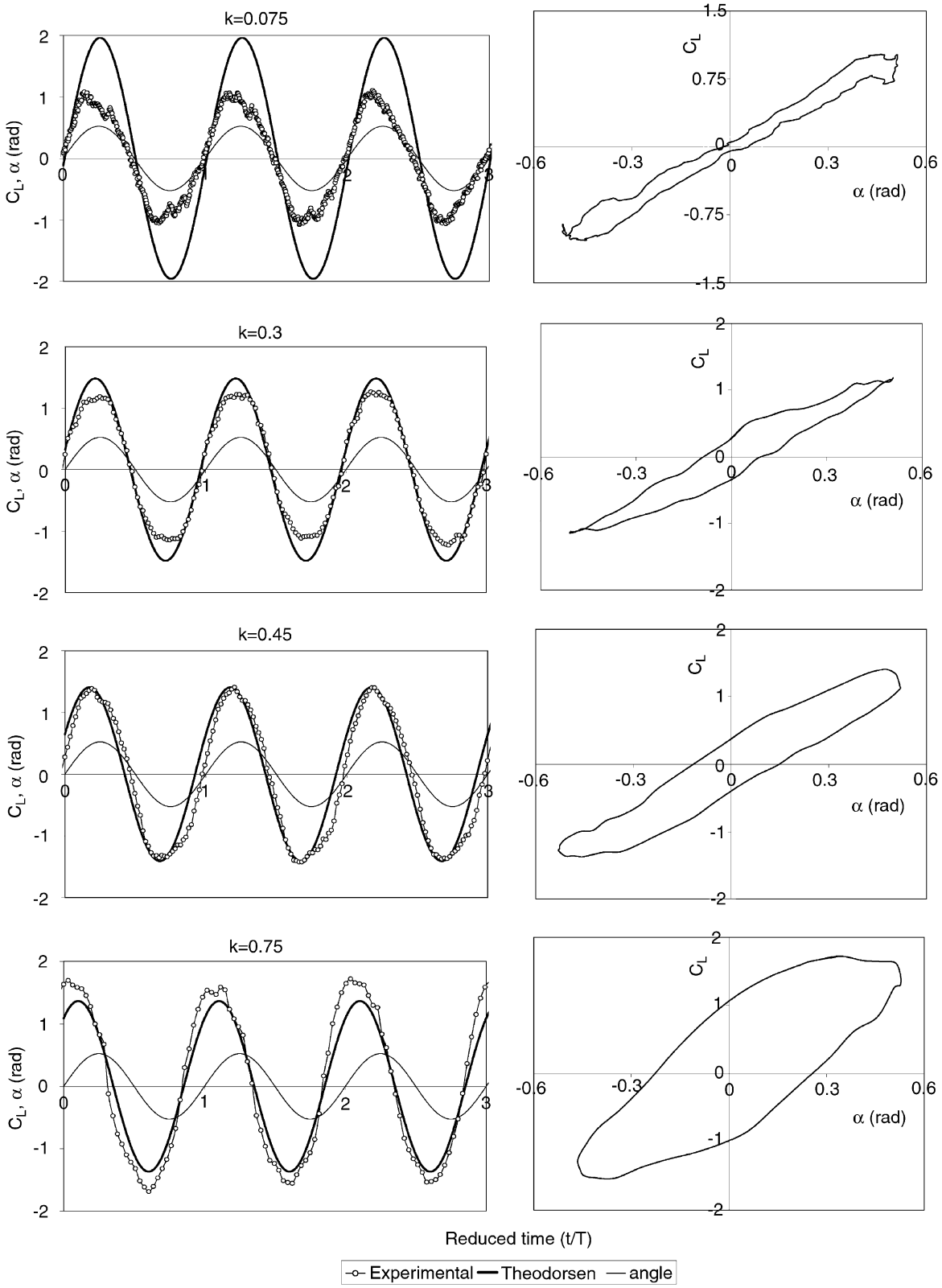

Fig. 7. Lift force measured for $0 \leqslant k \leqslant 0.75$, $-30^\circ \leqslant \alpha \leqslant 30^\circ$, $\mathrm{Re} = 10^4$. Left-hand side—against reduced time, Right-hand side—hysteresis plots (clockwise orientation).

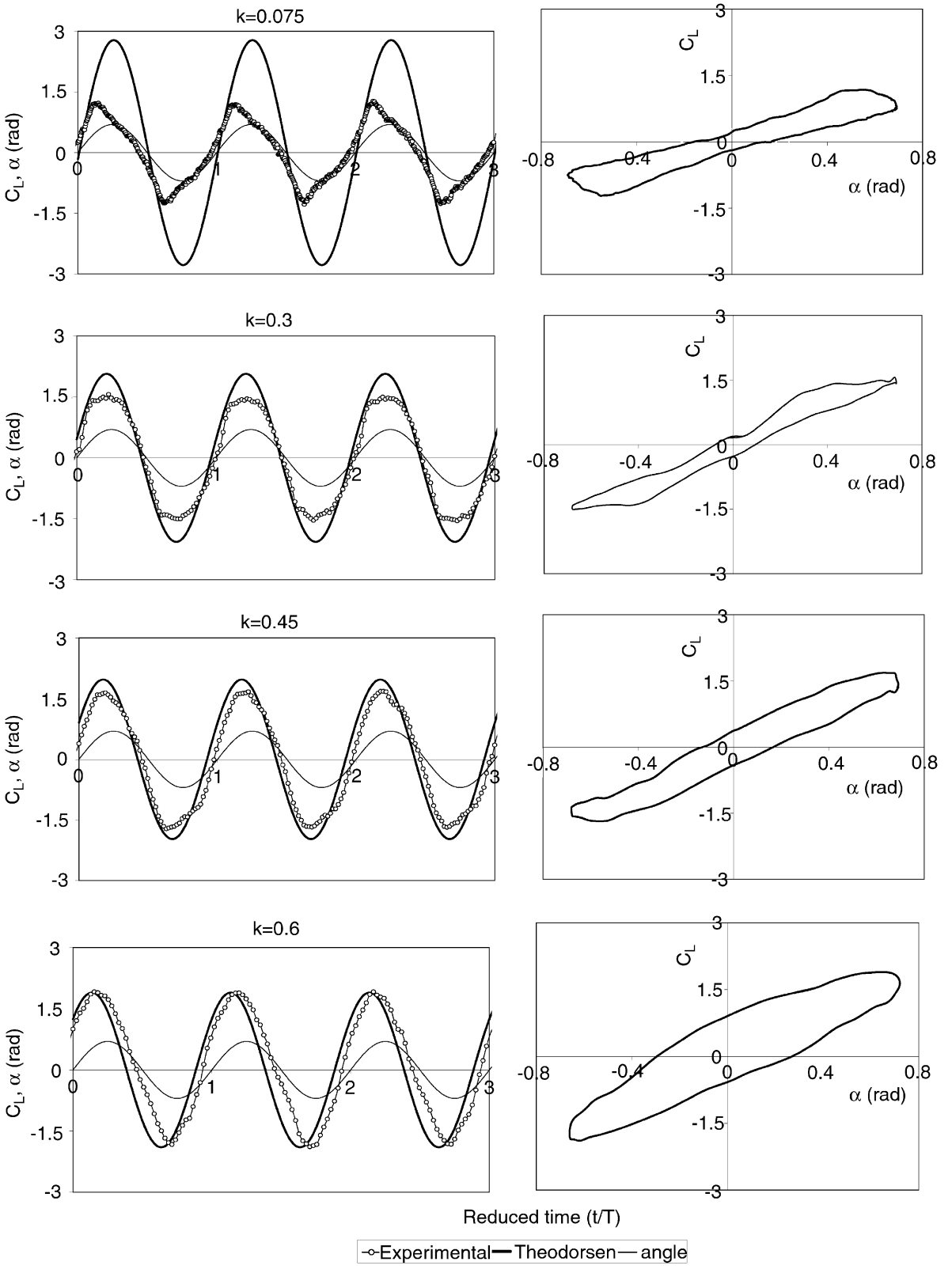

Fig. 8. Lift force measured for $0 \leqslant k \leqslant 0.6$, $-40^\circ \leqslant \alpha \leqslant 40^\circ$, $\mathrm{Re} = 10^4$. Left-hand side—against reduced time, Right-hand side—hysteresis plots (clockwise orientation).

dynamic stall vortex shed later relative to the angle of attack. The stall was therefore delayed—similarly observed here for $k = 0.3$. At even higher values of k, Akbari and Price observed that vortices did not have time to shed before the cycle was over and remained attached to the surface of the wing even at low angles of attack. This created a net pressure on the wing surface in a sense that aided the motion of the wing. This has also been observed here since significantly high phase lead of lift over angle of attack occurs at high values of k. This means that unsteady effects from previous cycles have an effect on the current cycle. As a result, the lift force is *advanced* by the unsteady effects, and has a substantial lead over the angle of attack. This concept will be revisited in Appendix A.

As with the $\pm 10^\circ$ results, Theodorsen's prediction appears to overestimate the lift force at low values of k. Also, similar to before, at low values of k, the theoretical prediction indicates a slight lag of the lift force behind the angle of attack, while the experimental results indicate a small lead of the lift force over the angle of attack. At $k = 0.9$ for $\pm 20^\circ$ peak angle of attack, theoretical predictions, as before underestimate the magnitude of the lift and overestimate the phase lead of the lift over the angle of attack, although the measured phase lead of the lift appears to be greater than for the $\pm 10^\circ$ case. It is reiterated here that physical limitations prevented an investigation of $k = 0.9$ for $\pm 30^\circ$ peak angle of attack. However, at $k = 0.75$, the measured lift appears to have a greater phase lead over the angle of attack as compared to Theodorsen's prediction.

Although physical limitations restricted the investigation at $\pm 40^\circ$ peak angle of attack to a maximum reduced frequency of $k = 0.6$ (see Fig. 8), clear trends are still observable. At $k = 0.075$, stall of the wing occurs at approximately 30°. This is at 75% of peak angle of attack as compared to 95% for $\pm 20^\circ$ and 90% for $\pm 30^\circ$ peak angle of attack. Increasing k again sees the stall apparently delayed and smoother lift plots and hysteresis loops as a result. At $k = 0.3$, the phase lead of the lift over the angle of attack is almost negligible. This observation combined with the earlier stall observation at $k = 0.075$ suggests an earlier relative shedding and therefore a larger relative effect of the dynamic stall vortex at this higher peak angle of attack.

Considering Theodorsen's prediction, the familiar over-estimate of the lift magnitude again exists at the lowest value of k. The error has expectedly increased due to the higher angle of attack, and therefore greater distance from the applicable range of Theodorsen's theory. The smallest discrepancy between Theodorsen's theory and experimental results occurs at the greatest reduced frequency of $k = 0.6$. Of great interest will be to observe if the lead of the lift over the angle of attack is greater than Theodorsen's predictions at higher values of k, as observed with the $\pm 30^\circ$ results.

For all experimental results, the peak lift value appears to increase with increasing reduced frequency k. Theodorsen's predictions do not support this observation, and rather reveal a decreasing peak lift with increasing reduced frequency (a result of a greater downwash correction for a higher lift force produced). This indicates that the correction to the angle of attack calculated by Prandtl's lifting line theory might not be accurate for a pitching wing, overcorrecting for high reduced frequencies, and undercorrecting for low reduced frequencies. Fig. 9 plots $C_{L,\max}/\alpha_{\max}$ against k for the four different maximum angles of attack. These curves summarize the magnitude differences between Theodorsen's results, experimental results and also CFD results (CFD results are separately presented in Appendix A). The results are consistent for all four cases of differing peak angles of attack and reveal excellent agreement between all three results around $k = 0.6$. Below $k = 0.6$, Theodorsen's results clearly estimate a higher lift force than both the experimental and CFD results. Above $k = 0.6$, the reverse appears to be true, as the experimental results show a higher respective lift force generated when compared with the other results. As with the curves presented in Figs. 7 and 8, high reduced frequencies were not measurable for peak angles of attack of 30° and 40°, however the results show strong signs of repeating similar patterns to those established at peak angles of attack of 10° and 20°.

At higher reduced frequencies it is proposed that vortex generation and shedding that may be possibly increasing the lift generated, as supported by the experimental results, cannot be captured by Theordorsen's theory. The CFD results, which model to some extent the major vortex effects, are closer to the experimental results. The smaller discrepancy between the CFD and experimental results is most probably attributed to excessive downwash corrections applied to the 2-D CFD simulations.

The implications of the magnitude discrepancies are not so serious from a phase point of view since the predicted phase difference is not very sensitive to changes in the simulated peak angle of attack, and only significantly change with reduced frequency.

4.2. Phase difference comparison

The trends observed in the phase difference were similar for all peak angles of attack greater than the static stall angle of 15°. By measuring and averaging the reduced phase difference measured as a portion of reduced time, plots of reduced phase difference with reduced frequency were generated and are presented in Fig. 10. (Reduced phase difference $= \eta/T$, where η is the phase difference in seconds measured at 0° angle of attack, and T is the time period of

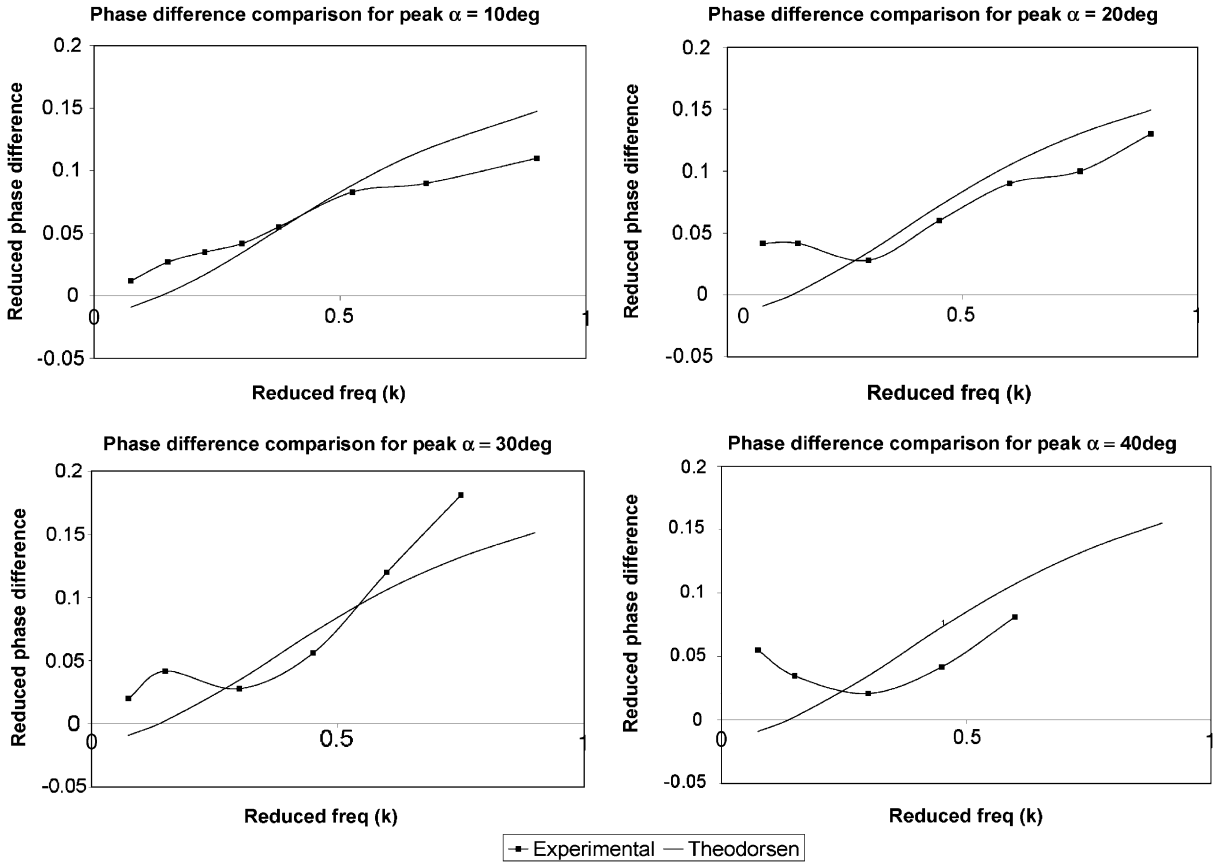

Fig. 9. k versus $C_{L,\max}/\alpha_{\max}$, for 10°, 20°, 30° and 40° peak angle of attack, comparing Theodorsen's results, experimental results and CFD results.

oscillation). It should be mentioned that experimental lag caused by the sensing equipment was too small for detection and was therefore considered negligible.

In Theodorsen's prediction of the phase difference between lift force and angle of attack a slight lag is seen at very low values of k, with an almost linear increase in the phase lead as k increases. This increasing trend is almost identical regardless of the peak angle of attack.

Experimental results appreciably differ. All results except for the $\pm 10^\circ$ plot (where dynamic stall effects are minimal) reveal general similarities. From $k = 0.1$, to $k = 0.3$, the reduced phase lead decreases slightly. For reduced frequencies greater than $k = 0.4$, the phase lead significantly increases with reduced frequency. By recognizing observations made by Akbari and Price (2003), the decreasing phase lead between $k = 0.1$ and $k = 0.3$ can be attributed to the complete formation of a vortex from the trailing edge during the return cycle of motion. Providing a suction effect, this translates into a superimposed delay in the reduction of lift while the angle of attack is approaching 0°. Above $k = 0.4$, the formation of the trailing edge vortex is reduced due to the presence of lingering leading edge vortices that do not have time to shed in the fast oscillation. The pressure distribution instead promotes motion and therefore increases the phase lead of the lift force over the angle of attack. The phase difference observations therefore further support the dynamic stall vortex effects observed by Akbari and Price (2003) and show that similar mechanisms may be occurring despite slightly different types of motion. To test this, numerical simulations of the experimental investigation have been carried out and presented in Appendix A. The numerical simulations provide a way to observe the pressure contours around the oscillating wing, to see if the dynamic phenomena observed by Akbari and Price are similarly occurring here.

Further to note is that the phase lead appears to increase slightly with increasing peak angle of attack. For pitching motion between $\pm 30^\circ$, and to a lesser extent $\pm 20^\circ$, the rate of increase in phase lead at high k appears faster than Theodorsen's predicted phase lead. This may be explained by analysing the circulatory and noncirculatory components

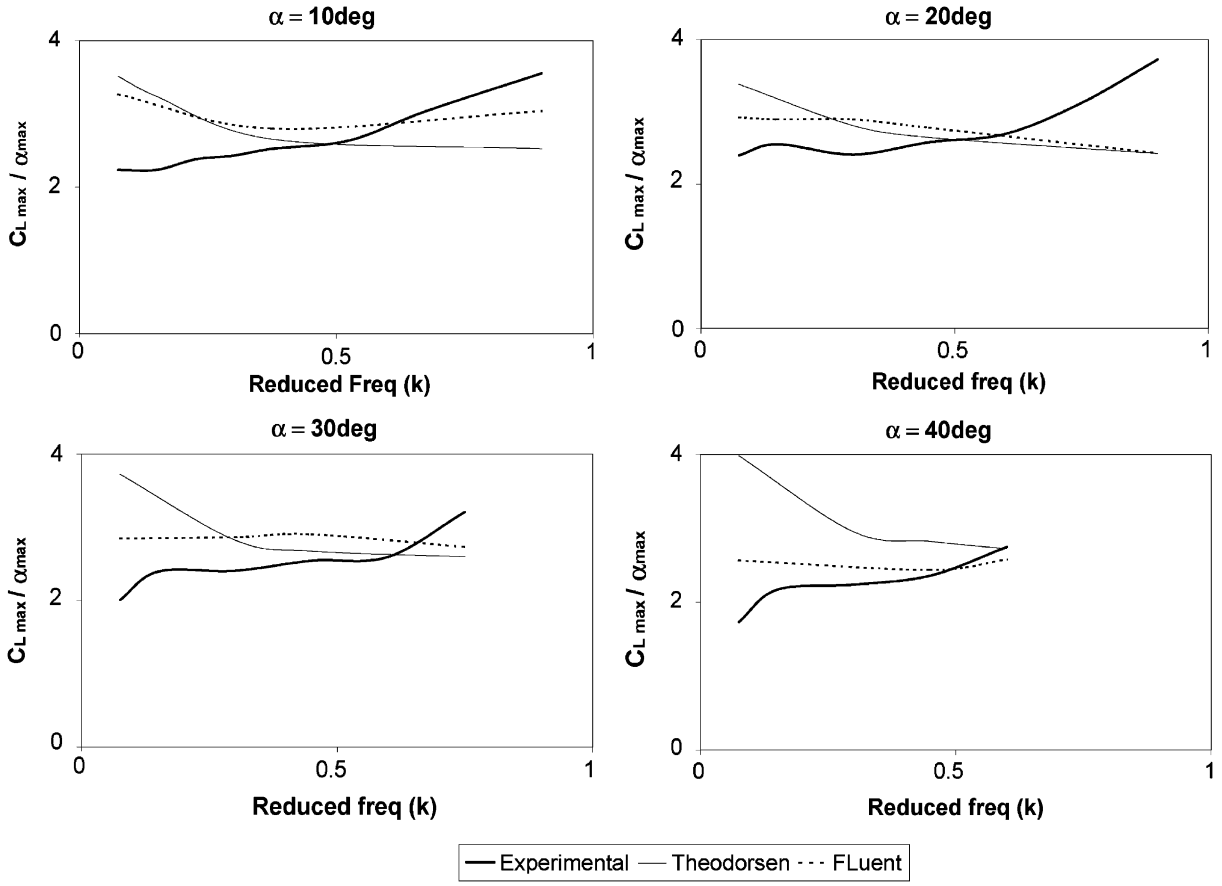

Fig. 10. Phase difference plotted against reduced frequency compared with Theodorsen's predicted phase difference calculated from Eq. (5d).

of Theodorsen's predicted lift force. Plots of Eqs. (5b), and (5c) in Figs. 11(a) and (b) reveal a larger relative influence of the circulatory force component and almost no influence from the noncirculatory force component at low k as opposed to a higher noncirculatory influence at high k.

It is therefore clear that at high reduced frequencies, the rate of increase in the predicted phase lead is a result of the increasing influence of the noncirculatory component or force due to the motion of the wing itself. The increasingly larger phase lead observed experimentally at high k and high peak angle of attack could therefore be due to the dynamic stall vortices observed by Akbari and Price—creating an extra phase lead in addition to the phase lead due to the noncirculatory or added mass effects.

At low values of k, the difference in sign between Theodorsen's predicted phase difference the measured phase difference may be due to geometry effects, and/or the thickness and profile of the wing. Since Theodorsen's model assumes a flat plate, the associated noncirculatory effects are very small at low values of k as shown in Fig. 11(a). A physical wing thickness and profile may increase the noncirculatory effects substantially enough to create a small phase lead of the lift force over the angle of attack—as observed in all experimental results at low values of k.

4.3. Summary of observed trends

The lift force has shown high levels of repeatability between cycles, even when varying between high angles of attack. Oscillating the wing has also created lift forces far in excess of the static stall lift (see Fig. 4). Varying the reduced frequency and peak angle of attack has led to observations of several trends.

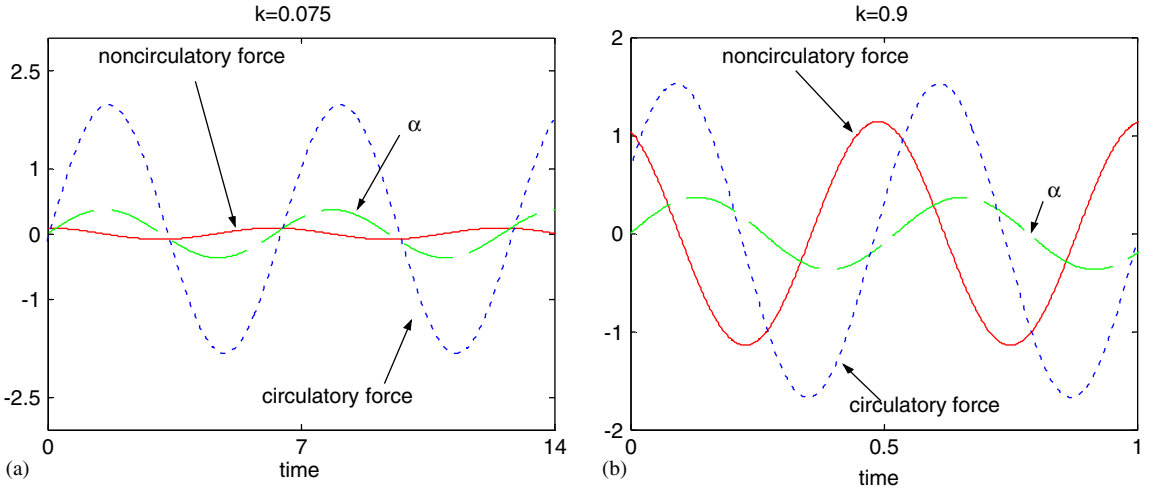

Fig. 11. (a) C_L components at low reduced frequency, (b) C_L components at high reduced frequency.

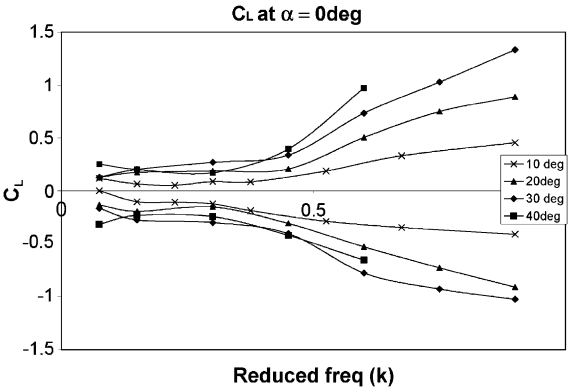

Fig. 12. Coefficient of lift measured at 0° angle of attack for various k, and peak angle of attack. Negative curves are generated when the AOA is decreasing, positive curves are generated when the AOA is increasing.

(i) *Reduced frequency k*. From the experimental results obtained, the reduced frequency appears to be the most influential parameter on the final lift force generated. Results indicate that a higher reduced frequency is associated with a slightly higher peak lift generation and a smoother lift curve. Increasing k generally increases the phase lead of the lift over the angle of attack, however over a small range of k from $k = 0.3$ to 0.45, the phase has been observed to decrease before increasing again.

(ii) *Peak angle of attack*. As expected, larger peak angles of attack have enhanced dynamic stall phenomenon experienced by the wing. Increasing the peak angle of attack beyond the static stall limit clearly results in changes in the lift force and hysteresis loops. There also exist small signs that larger peak angles of attack are associated with a greater phase lead of the lift over the angle of attack at high values of k.

Fig. 12 shows the lift coefficient measured at 0°angle of attack. The results give an idea of the symmetry between positive and negative cycles, indicating strong repeatability. It also shows that increasing the reduced frequency and increasing the peak angle of attack increases the lift generated when the angle of attack is 0°.

5. Concluding remarks

The unsteady lift for wing pitching in simple harmonic motion in an incompressible flow has been analysed using Theodorsen's thin airfoil theory and also experimentally. A comparison of results has shown encouraging correlation in terms of phase difference between the lift coefficient and the angle of attack. However, experimental results have revealed a decrease in the phase lead between $k = 0.3$ to 0.45 followed by a faster increase in the phase lead at higher k.

Prandtl's lifting line theory has been used to correct the angle of attack of the 2-D theoretical prediction for a comparison with 3-D experimental results. The correction appears to underestimate the downwash at low reduced frequencies and overestimate the downwash at high reduced frequencies creating significant discrepancies with experimental results in the magnitude of the generated lift. It has also been observed that dynamic stall effects and hysteresis in the shedding of dynamic stall vortices have significant effects on the generated lift force that Theodorsen's model cannot predict.

The reduced frequency appears to have the most influence on the generated lift force in terms of phase difference and deflections in the lift curve caused by dynamic stall effects, while increasing the peak angle of attack appears to amplify dynamic stall effects.

Referring to the original motivation for the investigation, a comfort control system should remain robust to the small variations in force caused by dynamic stall vortices. However, the system may be improved by incorporating the phase difference information into the model.

It is worth mentioning here that only the sinusoidal lift force is investigated in this paper, which makes the analysis of frequency-dependent phase difference and amplitude easier. Also Theodorsen's result, used for comparison, is based on the linear potential flow theory, and the Fourier transformation promises the conversion of the result from the frequency to the time domain. As the true wing motion induced by a comfort controller would not be simple harmonic, and nonlinear behaviour of the pitching wing dynamics may not be ignored, future work should focus on the lift force produced by arbitrary wing motion in which case, the mathematical model will appreciably differ.

Acknowledgements

The research carried out in this paper was funded by an ARC Grant at the University of Western Australia (ARC Grant No. LP0219249).

The authors would also like to acknowledge the advice and opinions received from Seastate Pvt. Ltd. during technical discussions which defined some of the objectives of the research project.

Appendix A

A.1. CFD comparison

Dynamic phenomena observed in the lift plots and hysteresis plots of Section 4.1 were explained with the aid of observations of vorticity plots simulated by Akbari and Price (2003). To bring further credibility to these explanations, several numerical simulations were carried out, from which pressure contours around the wing could be simulated during an oscillation cycle. The numerical simulations carried out here are in good agreement with the experimentally measured results. Limitations in computing power have limited the numerical simulation to 2-D; therefore Prandtl's lifting line theory has been used once again to correct the incident angle of attack for comparison with 3-D measured results.

The CFD package (Fluent) was used to perform the numerical simulation of an oscillating wing. Fluent uses the finite volume method and solves conservation equations for mass and momentum to determine the pressure distribution and therefore fluid dynamic forces on the wing as a function of time.

Choice of a suitable turbulent model is dependent on many factors ranging from flow characteristics to available computing power. Due to the limitations in computing power, only two models were realistically applicable for this project: the popular k–ε turbulence model [see FLUENT 6.1 Fluent User's Guide (2002, Chapter 10.2.5)], and the k–ω turbulent model [see FLUENT 6.1 Fluent User's Guide (2002, Chapter 10.2.8)]. Both turbulence models are two-equation models in which the solution of two separate transport equations allows the turbulent velocity and length scales to be independently determined. With advantages and disadvantages existing for each model, the k–ω model was chosen due to its accuracy with transitional flows.

Gambit 2.0 was used to create the discretized domain, or mesh and Fluent's moving deforming mesh (MDM) function was used to produce the wing motion. Between iterations, the MDM function deforms or re-meshes grid cells as the wing pitches back and forth. This process is often susceptible to creating highly skewed cells, which in turn causes inaccurate solutions and slow convergence. Deforming cells around the surface of the wing and the trailing edge—areas with the steepest pressure gradients that require the highest-quality cells, would be especially undesired. To deal with this problem, a circular region around the wing was created with its centre point at one-quarter chord length. An interface between the interior of the circle and cells external to the circle was also established. This whole circular region was set up to pitch and only cells externally adjacent to the interface were deformed and re-meshed. This implied that high-quality boundary layer cells remained undeformed inside the circle in the critical flow areas around the wing (see Figs. 13(a–c)). This technique also significantly allowed the placement of a boundary layer around the wing.

The in-built Gambit sizing functions, and boundary layer ratios were adjusted and tuned until the mesh exhibited grid independence. The resulting mesh had excellent quality in terms of skewness: 99% of cells exhibited a skewness less than 0.5, and no cells had a skewness greater than 0.7. The total number of cells amounted to 29 082.

Comparisons between the mesh used and conventional deforming meshes without zones reveal much higher accuracy and faster convergence for the circular zoned mesh. Several different circular zoned mesh versions were tested for grid independence before the final mesh was chosen—displayed in Fig. 13(a).

A.2. Numerical simulation results

The time step for the unsteady sinusoidal pitching simulations was considered for both computing time, and accuracy. Time step independence was achieved at $0.002T$. A time step less than $0.002T$, where T is the pitching period, did not significantly alter the results in light of the extra computing time required. At each time step, a maximum of 20

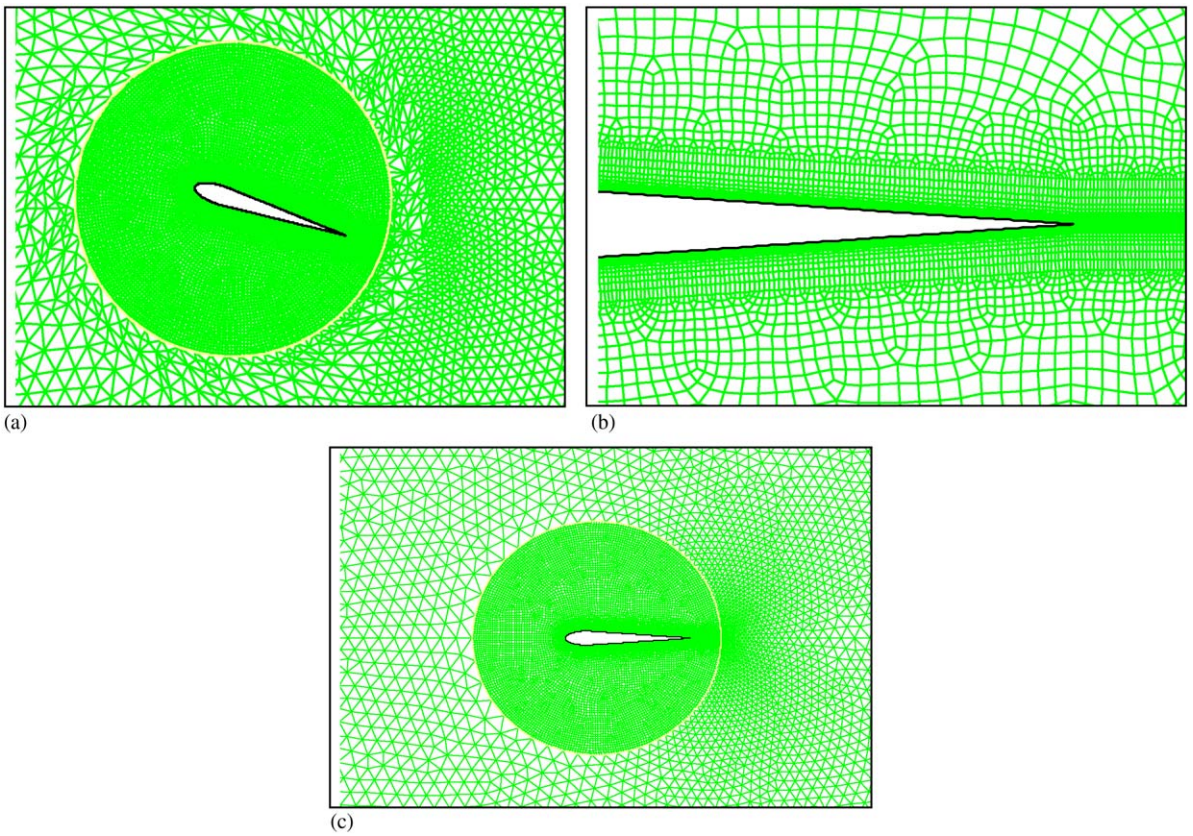

Fig. 13. (a) Simulation mesh constructed in GAMBIT. (20 000 cells), (b) boundary layer mesh at trailing edge, (first row size: 0.01 mm, growth factor: 1.3, boundary layer thickness: (20 rows, 6 mm) and (c) deformed mesh during oscillation. (maximum skewness: 0.7).

iterations was chosen; however, during simulations, it was observed that the solution would converge below residual values of 0.1% after only 10 iterations at every time step.

Since it was observed that motion at larger peak angles of attack were associated with larger scale dynamic stall phenomena, numerical simulations were carried out for $k = 0.075$, 0.45, and 0.6 for a 40° peak angle of attack. Plots of numerically simulated lift coefficient against reduced time and hysteresis loops are compared with the corresponding experimental results and are shown in Fig. 14 for the three reduced frequencies. The Reynolds number was again set at 10^4.

From Fig. 14, predictions from Fluent's numerical simulation appear to have excellent correlation with experimental results. As with experimental results, strong repeatability exists between cycles, along with symmetry between positive and negative cycles. At the lower reduced frequency of $k = 0.075$, the numerical simulation predicts an almost identical

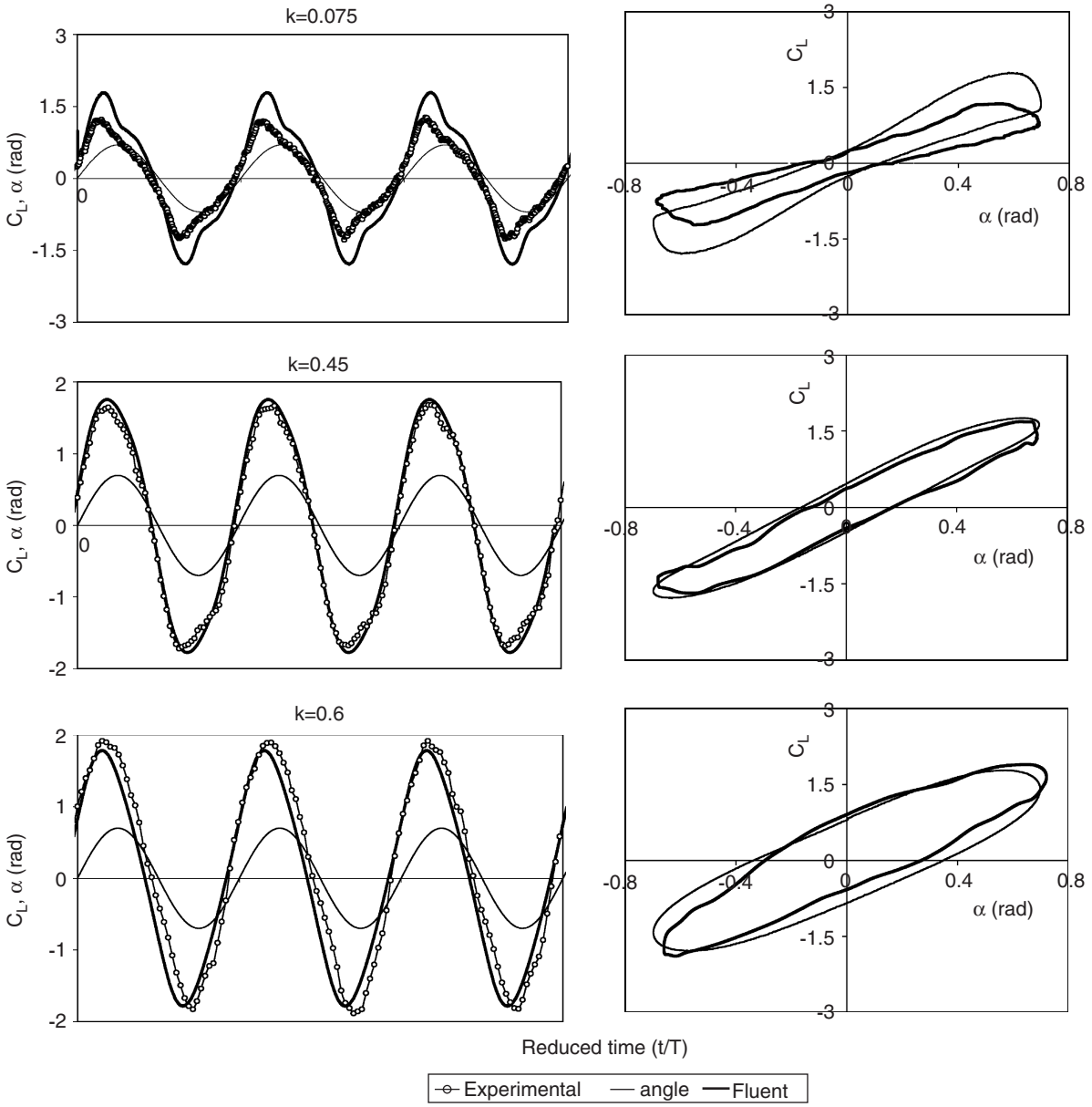

Fig. 14. CFD predicted lift coefficient compared with experimentally measured lift coefficient for $k = 0.075$, 0.45 and 0.6. Coefficient of lift against reduced time (l.h.s), hysteresis loops (r.h.s). Fluent lift coefficient: —, experimental lift coefficient: ▬.

phase lead of the lift coefficient over the lift force. Stall of the wing occurs at approximately the same angle of attack of $\pm 30^{\circ}$, while a recovery of lift force following the stall also occurs at approximately the same angle of attack of $\pm 40^{\circ}$. The magnitude of the lift coefficient predicted by the numerical simulation, however, overestimates the measured lift force. This can most likely be attributed to inaccuracies in the imposed downwash correction as assumed in the comparison with Theodorsen's model. The hysteresis loops at $k = 0.075$ also show a high correlation with experimental results. The thickness as well as the general shape of the loop is very similar. It is only the discrepancy in the magnitude of lift that causes a slight discrepancy in the orientation of the loop.

At $k = 0.45$, the agreement between experimental and numerical results is even greater. At the higher oscillating frequency the downwash correction applied to the numerical results appears to be more accurate. Combined with accurate numerical phase lead predictions, and trends in the hysteresis loop, the numerical result is almost identical to the experimentally measured result. Although not visually obvious in Fig. 14, analysis of larger figures, allows one to see a slight deflection in the return cycle of the lift curve against reduced time. This supports the experimentally measured deflection in the return cycle of the lift curve which is more obvious in Fig. 14.

At $k = 0.6$, the agreement between numerical and experimental results is again very close. The numerically generated lift curve is very smooth with no apparent deflections during the return cycles. The numerically predicted magnitude of the lift coefficient is also very close the experimentally measured lift coefficient with only a slight underestimation error. Hysteresis loops generated by both numerical and experimental data have increased in thickness and changed orientation similarly as compared with hysteresis loops from $k = 0.45$.

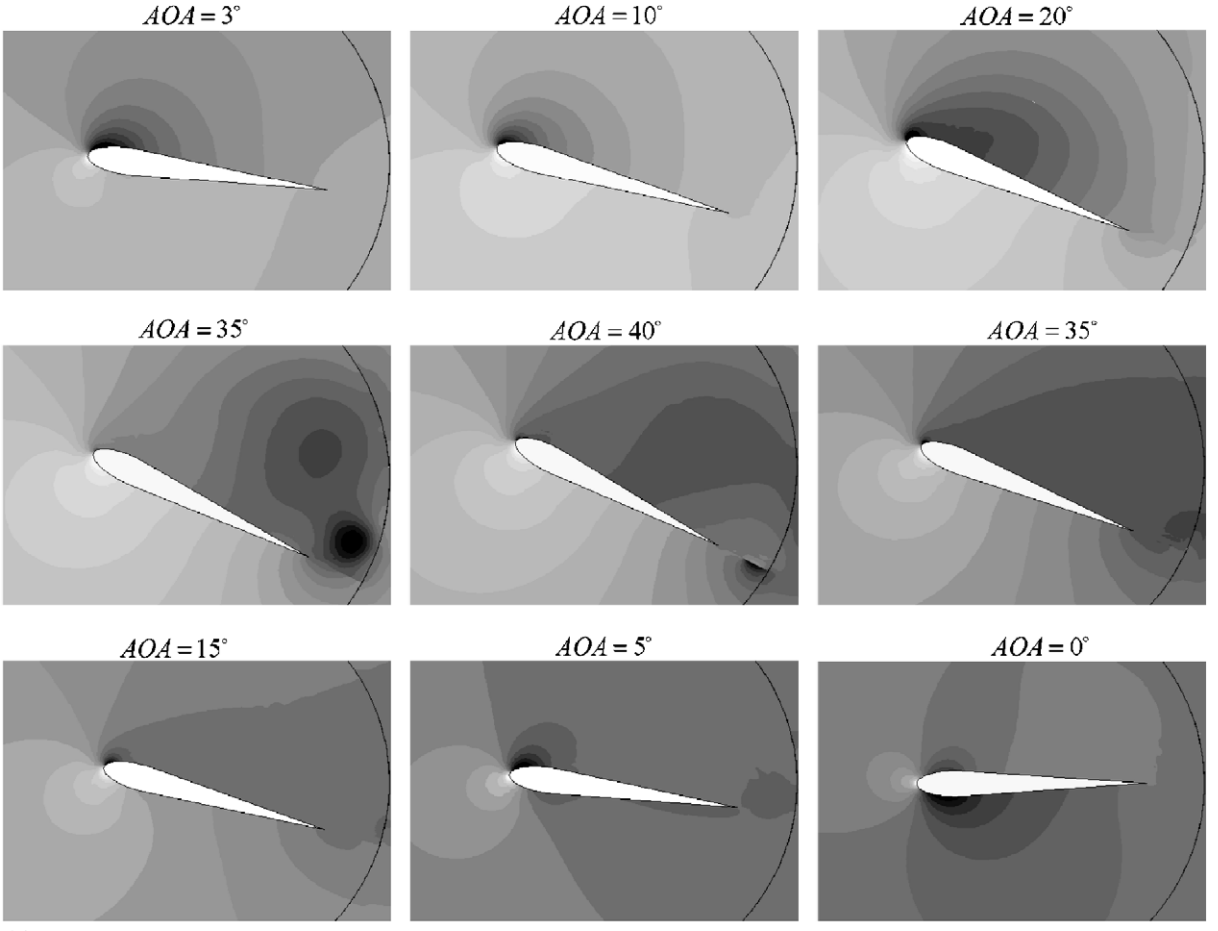

Fig. 15. Pressure contours for positive cycle of oscillation: (a) $k = 0.075$, (b) $k = 0.45$ and (c) $k = 0.6$. Dark shaded regions are areas of negative pressure, light shaded regions are areas of positive pressure.

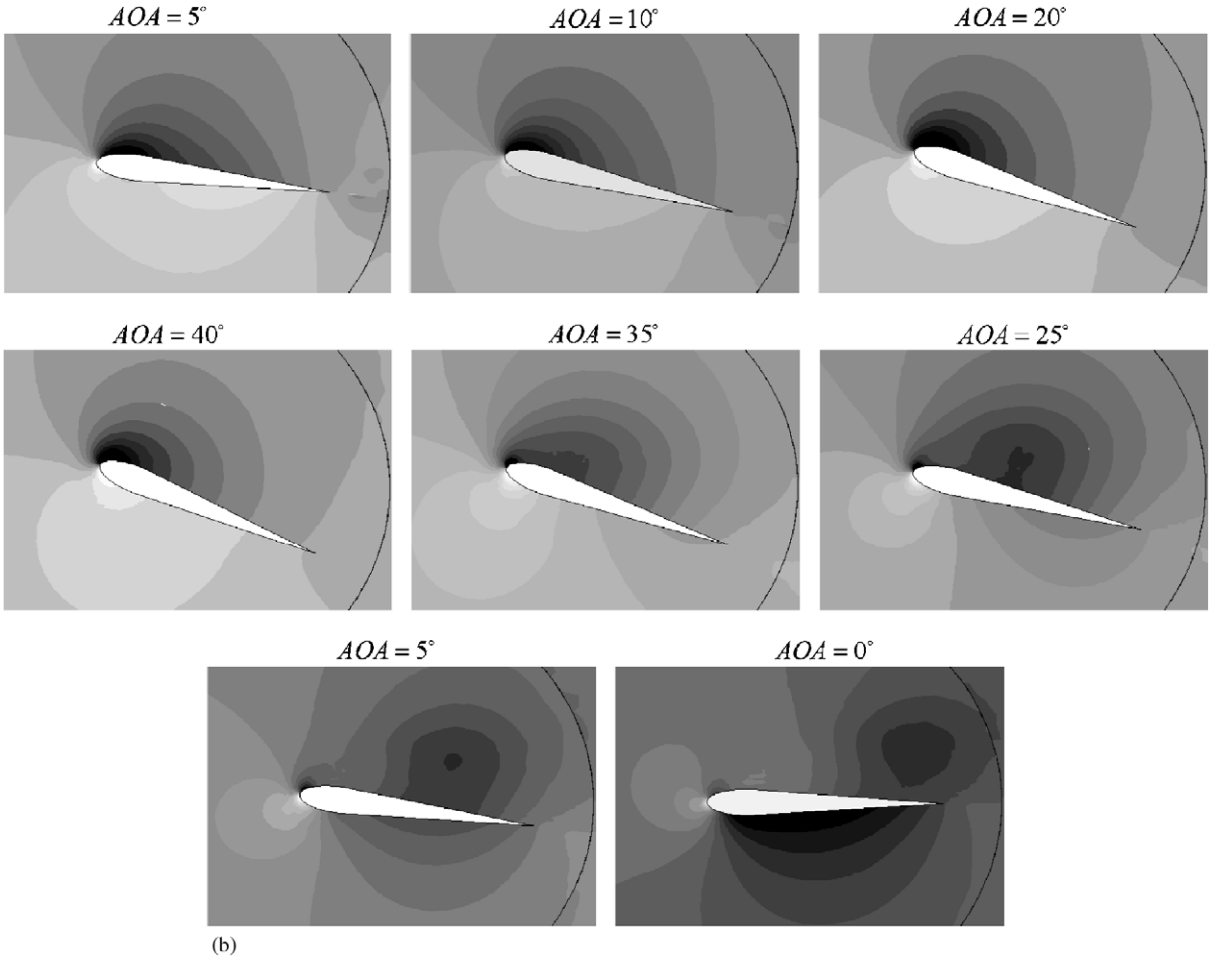

Fig. 15. (*Continued*)

From these results, the numerical simulations provided by Fluent appear valid and other functions from Fluent can therefore be utilized to analyse the flow.

As mentioned previously, the numerical simulation carried out assumed a 2-D flow field. Although Fluent is capable of modelling 3-D flow fields, computing requirements downgraded the simulation to 2-D. Similarly, more advanced features of Fluent that can more accurately predict complicated flows were not utilized due to the high computing requirements. A brief analysis of Fig. 14 would suggest that the higher-level functions within Fluent are not necessary in this situation since simple 2-D simulations have captured the main characteristics of the experimental results. However, vorticity snapshots of the flow in the detail provided by Akbari and Price (2003) are not possible with the simplifications applied to the simulations here. Nevertheless, the pressure contours around the wing provide good indicators to the location of forming and shed vortices. Figs. 15(a–c) display the pressure contours around the wing at various angles of attack for $k = 0.075$, 0.45, 0.6, respectively.

For $k = 0.075$, high-pressure regions are clearly present beneath the wing while low-pressure regions exist above the wing. At 20°, the onset of stall is apparent as the low-pressure region near the leading edge looks to be pulling away from its centre. At 35°, a vortex from the leading edge and trailing edge has been shed and moved away from the wing surface. This corresponds with the drop in lift observed in Fig. 14 at the same angle of attack. From the peak angle of attack of 40°to $AOA = 15°$, the vortices have moved away and a low-pressure region has re-developed above the wing, possibly due to another vortex forming on the surface. This corresponds with the deflection in the lift curve starting at 40°. At $AOA = 5°$, another vortex has shed from the trailing edge, and a low pressure region is forming beneath the wing. The net pressure on the wing at this stage is in a negative sense. At $AOA = 0°$, the low-pressure region beneath the wing has obviously formed, and the lift force is negative.

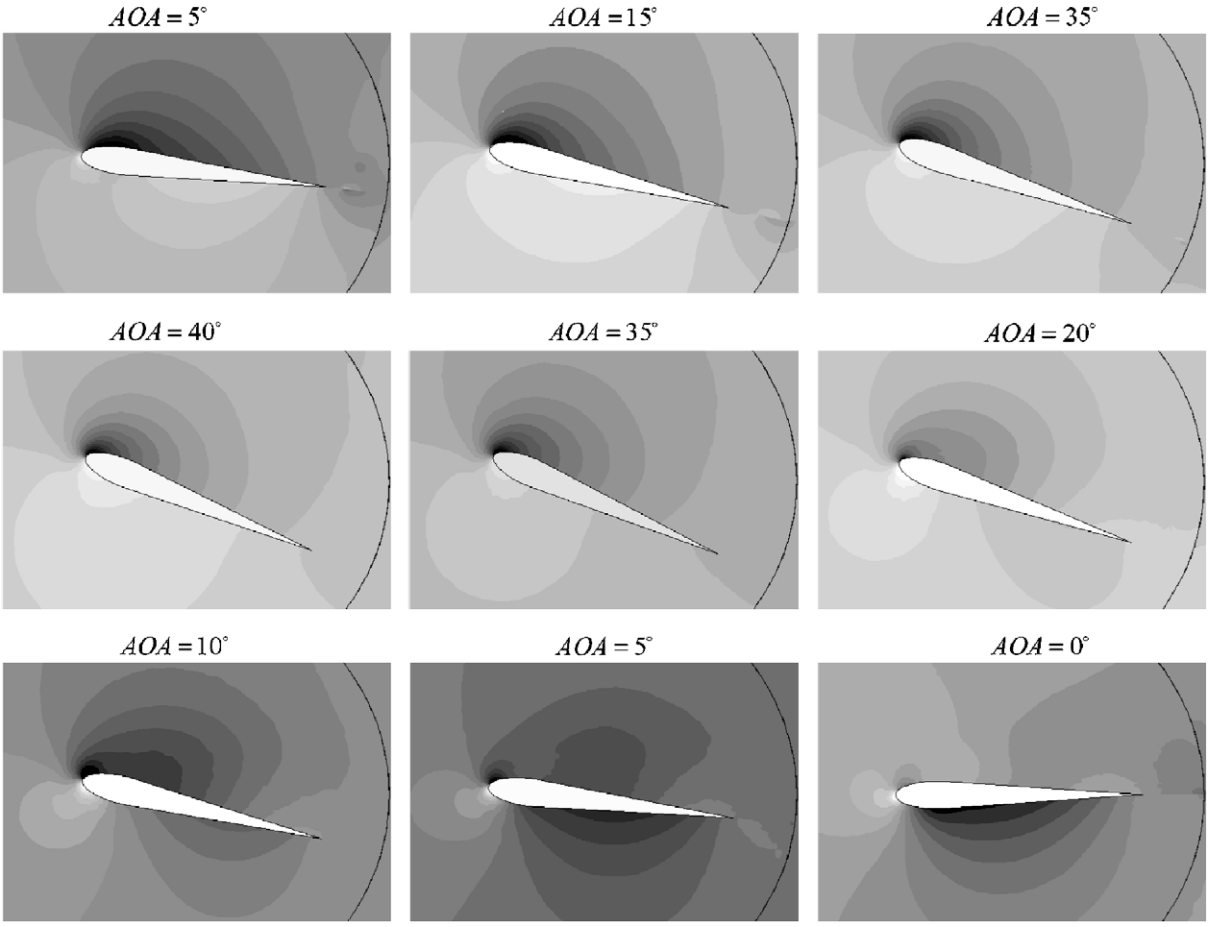

(c)

Fig. 15. (*Continued*)

For $k = 0.45$ (see Fig. 15(b)), the flow appears to remain attached throughout the upstroke. The positive pressure area is clear to see steadily increasing beneath the wing, while the same occurs for a negative pressure region above the wing. When the wing reaches the maximum angle of attack of 40°, the flow is still attached. As the downstroke begins, a vortex (dynamic stall vortex) begins to shed from the leading edge as seen in $AOA = 35°$. At $AOA = 25°$ the vortex can be seen to be moving down the surface of the wing. Its presence at this stage creates a large low pressure region on the upper surface of the wing effectively creating a suction effect and as a consequence a slight deflection in the lift curve as seen in Fig. 14. As described in Section 3.2, this is the reason behind the apparent decrease in the lead of the lift force over the angle of attack between $k = 0.3$ and 0.45. The suction force from the leading edge vortex effectively creates a delay in the decay of the lift force as it is decreasing. As the wing's angle of attack decreases further to 5°, the vortex begins to shed away from the wing surface and a low pressure region begins to form beneath the wing. At $AOA = 0°$, the leading edge vortex has shed. Its suction effect diminishes and the net pressure on the wing is in a negative sense.

For all of the upstroke and half of the downstroke at $k = 0.6$ (see Fig. 15(c)), the pressure contours reveal nothing particularly interesting in terms of formed or shed vortices. It is not until $AOA = 20°$ during the downstroke that a vortex forming on the leading edge can be visibly seen. The formation of this leading edge vortex is occurring much later than in the cases of $k = 0.45$ where it formed at 35° during the downstroke, and $k = 0.075$ where it formed at 20° during the upstroke. This is a good example of the hysteresis or lagging effects caused by the faster motion. At these higher speeds, vortices have less time to form and shed with respect to the relative motion. For $k = 0.45$, the leading edge vortex created a suction effect on the upper surface of the wing that corresponded with a deflection in the return cycle of the lift curve. In this case, the leading-edge vortex takes its position on the upper surface of the wing much later at $AOA = 5°$. By this time, a negative pressure region has already formed beneath the wing, effectively cancelling out the

effects of the vortex above the wing. At 0°, the leading edge vortex has moved away from the wings surface, and a strong negative pressure region beneath the wing is well estabished. The wing is already producing substantial negative lift.

The pressure contours simulated by Fluent have contributed to the explanations behind the changes in the lift force observed experimentally. Although the investigated motion differs from that of Akbari and Price (2003) similar phenomena have been observed—particularly relating to hysteresis of vortex shedding and their effects on the lift force.

References

Akbari, M.H., Price, S.J., 1999. Simulation of the flow over elliptic airfoils oscillating at large angles of attack. Journal of Fluids and Structures 15, 757–777.

Akbari, M.H., Price, S.J., 2003. Simulation of dynamic stall for a NACA 0012 airfoil using a vortex method. Journal of Fluids and Structures 17, 855–874.

Bielawa, R.L., Johnson, S.A., Chi, R.M., Gangwani, S.T., 1983. Aeroelastic analysis for Propellers—Mathematical Formulation and Program User's Manual. N.A.S.A CR 3729.

Do, K.D., Pan, J., 2001. Smooth asymptotic robust fin roll stabilization of surface ships. In: Proceedings of the IASTED International Conference on Modeling Identification, and Control, February 19–22, 2001, Innsbruck, Austria.

Ericsson, L.E., Reding, J.P., 1972. Dynamic stall of helicopter blades. Journal of the American Helicopter Society 17, 785–796.

FLUENT 6.1. Fluent User's Guide, 2002. Leap Australia Pvt. Ltd.

Houghton, E.L., Carpenter, P.W., 2003. Aerodynamics for Engineering Students, fifth ed. Butterworth-Heinemann, Oxford.

Jones, R.T., 1939. The unsteady lift of a finite wing. N.A.C.A TN 682.

Jones, R.T., 1941. The unsteady lift of a wing of finite aspect ratio. N.A.C.A TN 681.

Khalil, H.K., 1996. Nonlinear Systems, second ed. Prentice-Hall, Englewood Cliffs, NJ.

Krstic, M., Kanellakopoulos, I., Kokotovic, P., 1995. Nonlinear and Adaptive Control Design. Wiley, New York.

Lamb, H., 1932. Hydrodynamics, sixth ed. Cambridge University Press, Cambridge.

McCroskey, W.J., 1973. Inviscid flowfield of an unsteady airfoil. AIAA Journal 11, 1130–1137.

McCroskey, W.J., 1982. Unsteady airfoils. Annual Review of Fluid Mechanics 14, 285–311.

Theodorsen, T., 1935. General theory of aerodynamic instability and the mechanism of flutter. N.A.C.A Rep. 496.

Tran, C.T., Petot, D., 1981. Semi-empirical model for the dynamic stall of airfoils in view of the application to the calculation of responses of a helicopter blade in forward flight. Vertica 5, 35–53.

Wernet, P., Koerber, G., Wietrich, F., Raffel, M., Kompenhans, J., 1996. Demonstration by PIV of the non-reproducibility of the flow field around an airfoil pitching under deep dynamic stall conditions and consequences thereof. Aerospace Science and Technology 2, 125–135.